

Single-nucleus RNA sequencing uncovers cell type-specific alterations in OSA-related liver injury

Received: 7 November 2025

Accepted: 25 February 2026

Published online: 02 March 2026

Cite this article as: Huang W., Wang C., Huang Y. *et al.* Single-nucleus RNA sequencing uncovers cell type-specific alterations in OSA-related liver injury. *Sci Rep* (2026). <https://doi.org/10.1038/s41598-026-42236-1>

Wen-Sen Huang, Chao-Qiang Wang, Yu-Zhen Huang, Jia-Min Luo, Chu-Dan Yang, Jie-Feng Huang, Li Lin & Li-Da Chen

We are providing an unedited version of this manuscript to give early access to its findings. Before final publication, the manuscript will undergo further editing. Please note there may be errors present which affect the content, and all legal disclaimers apply.

If this paper is publishing under a Transparent Peer Review model then Peer Review reports will publish with the final article.

ARTICLE IN PRESS

Single-nucleus RNA sequencing uncovers cell type-specific alterations in OSA-related liver injury

Wen-Sen Huang¹, Chao-Qiang Wang^{1,2}, Yu-Zhen Huang³, Jia-Min Luo¹, Chu-Dan Yang^{1,4}, Jie-Feng Huang⁵, Li Lin^{1,4}, Li-Da Chen^{1,4}

¹Department of Respiratory and Critical Care Medicine, Zhangzhou Affiliated Hospital of Fujian Medical University. Zhangzhou, Fujian Province, China.

²The Second Clinical Medical College of Fujian Medical University. Fuzhou, Fujian Province, China.

³Department of Pathology, Zhangzhou Affiliated Hospital of Fujian Medical University, Zhangzhou, Fujian Province, China.

⁴Sleep medicine center, Zhangzhou Affiliated Hospital of Fujian Medical University. Zhangzhou, Fujian Province, China.

⁵Department of Respiratory and Critical Care Medicine, the First Affiliated Hospital of Fujian Medical University. Fuzhou, Fujian Province, China.

Correspondence to: Li-Da Chen, email: 361328175@qq.com, fax number: +8605962081166, telephone: +8613960805535. Address: No 59, Shenglixiroad, Xiangcheng district, Zhangzhou, Fujian province, People's Republic of China, 363000.

Wen-Sen Huang, Chao-Qiang Wang, and Yu-Zhen Huang contributed equally.

Abstract

Chronic intermittent hypoxia (CIH), a hallmark feature of obstructive sleep apnea (OSA), is strongly implicated in the development of hepatic injury. However, the cellular mechanisms underlying CIH-induced liver dysfunction remain poorly understood. This study aimed to systematically characterize hepatic cellular responses to CIH at single-nucleus resolution. A rodent model of CIH was established and subjected to histological and transcriptomic analyses. Single-nucleus RNA sequencing (snRNA-seq) was performed to delineate transcriptional alterations across liver cell populations. Differentially expressed genes (DEGs) and pathway enrichment analyses were conducted to identify key biological processes and signaling networks affected by CIH exposure. CIH exposure resulted in marked hepatic injury characterized by spotty necrosis and prominent infiltration of inflammatory cells. SnRNA-seq identified ten major liver cell types with stable composition but revealed extensive transcriptional reprogramming across multiple hepatic subpopulations. CIH suppressed PPAR signaling and fatty acid metabolism in hepatocytes and hepatic stellate cells and activated AMPK and PI3K-Akt pathways related to stress response and fibrogenic processes. Mononuclear phagocytes showed upregulation of NF- κ B signaling and complement/coagulation cascades. Endothelial cells exhibited changes in genes associated with cytoskeletal organization and tight junctions. T cell subpopulations displayed altered expression of genes involved in metabolic regulation and endoplasmic reticulum stress. This study provides the first

single-nucleus transcriptomic atlas of the liver under CIH, revealing cell type-specific molecular remodeling across hepatocytes, stromal, and immune cells. These findings elucidate the complex cellular interplay associated with CIH-induced hepatic injury and offer novel insights into potential therapeutic targets for OSA-related liver dysfunction.

Keywords: obstructive sleep apnea; chronic intermittent hypoxia; hepatic injury; single-nucleus RNA sequencing

ARTICLE IN PRESS

Introduction

Obstructive sleep apnea (OSA) is a common sleep disorder characterized by recurrent episodes of complete or partial upper airway obstruction during sleep, leading to chronic intermittent hypoxia (CIH) and sleep fragmentation. OSA has a worldwide prevalence of approximately 936 million people aged 30–69 years, with approximately 425 million people suffering from moderate to severe OSA¹. Growing evidence suggests that OSA is associated with systemic complications, such as liver damage, especially non-alcoholic fatty liver disease (NAFLD)^{2,3}. CIH is a major feature of OSA. Although several studies have investigated the mechanisms underlying OSA-related liver injury using CIH animal models^{4–6}, the precise pathways remain poorly understood. In particular, the molecular and cellular processes linking CIH to hepatic damage are still being elucidated.

Single-nucleus RNA sequencing (snRNA-seq) is a powerful technique that enables transcriptomic profiling at single-nucleus resolution, allowing the identification of cell type-specific gene expression patterns in both normal and diseased tissues⁷. Compared with conventional bulk RNA sequencing, snRNA-seq can capture cellular heterogeneity and rare cell populations, providing a more comprehensive understanding of tissue complexity^{8,9}. Moreover, unlike single-cell RNA sequencing (scRNA-seq), which requires viable whole cells, snRNA-seq isolates nuclei rather than intact cells, making it particularly suitable for frozen or fragile tissues where cell dissociation can lead to transcriptional artifacts or cell loss¹⁰. In recent years, snRNA-seq has been widely applied to

investigate the cellular and molecular mechanisms underlying various diseases, including cancer¹¹, metabolic disorders¹², neurodegenerative diseases¹³, and liver pathologies¹⁴. Despite these advances, snRNA-seq has not yet been utilized to explore the cellular landscape and molecular alterations in OSA-related liver injury.

In this study, we applied snRNA-seq to comprehensively characterize the liver at single-nucleus resolution in a CIH-induced rodent model of liver injury. Our aim was to uncover cell type-specific transcriptional alterations and potential molecular pathways involved in OSA-related hepatic injury, providing novel insights into the pathogenesis and identifying potential targets for therapeutic intervention.

Methods

Animals and subgroups

All animal procedures were approved by the Animal Ethics Committee of Fujian Medical University (IACUC FJMU 2022-0031) and conducted in accordance with institutional and national guidelines for the care and use of laboratory animals, following the ARRIVE reporting standards. Twelve male Sprague-Dawley rats (8 weeks old) were purchased from the Laboratory Animal Center of Fujian Medical University. The rats were acclimatized for one week under standard housing conditions (12:12 h light-dark cycle) with free access to food and water. After acclimatization, the rats were allocated into two groups via computer-based randomization: normoxia control (NC) and CIH, with $n = 6$ each

group.

Intermittent hypoxia (IH) exposure

The IH cycle consisted of four sequential phases, as previously described: a 120-second gradual decrease in oxygen concentration from 21% to 6%, followed by a 30-second period of sustained hypoxia at 6% O₂, a rapid 10-second reoxygenation back to 21%, and a 20-second normoxic phase¹⁵. Rats in the CIH group underwent daily 8-hour cyclic hypoxia, with the exposure scheduled from 08:00 to 16:00 during the light phase. Rats in the NC group were exposed to room air under normoxic conditions for the same daily duration. After 12 weeks of modeling, the animals were euthanized for liver sample collection via intraperitoneal injection of pentobarbital sodium (50 mg/kg).

Hematoxylin-eosin (HE) staining

Samples were fixed in 10% neutral-buffered formalin for 24 hours at room temperature, followed by dehydration through a graded ethanol series, clearing in xylene, and embedding in paraffin. Paraffin-embedded liver blocks were sectioned at 4 µm thickness using a microtome and mounted on glass slides. Sections were deparaffinized in xylene, rehydrated through a descending ethanol series to distilled water, and stained with hematoxylin for 5 minutes, followed by eosin for 2 minutes. Stained sections were dehydrated, cleared, and coverslipped with a mounting medium. Liver sections were examined under an Olympus BX50 optical microscope (Olympus, Tokyo, Japan) at 100× magnification, and histological scoring was performed by a pathologist blinded to the rats' group

assignments.

Nuclei Isolation and Sorting

From each group of six rats, three liver samples were randomly selected for downstream sequencing. Liver tissues were harvested and we washed them in pre-chilled PBSE (PBS with 2 mM EGTA) to remove blood and debris. We then isolated nuclei following the manufacturer's instructions for GEXSCOPE® Nucleus Separation Solution (Singleron Biotechnologies, Nanjing, China). After isolation, nuclei were resuspended in PBSE to a concentration of 10^6 nuclei per 400 μ l, filtered through a 40 μ m strainer, and enumerated using Trypan blue. To evaluate nuclei quality, the enriched nuclei were stained with DAPI (1:1,000; Thermo Fisher Scientific). Only nuclei with >80% integrity and <20% non-nuclear debris, with a total count exceeding 50,000 per sample, were used for downstream library preparation.

SnRNA-seq library preparation

The concentration of single-nucleus suspensions was set at $3-4 \times 10^5$ nuclei/mL in PBS and then loaded onto a microfluidic chip using the GEXSCOPE® SnRNA-seq Kit (Singleron Biotechnologies, Nanjing, China) according to the manufacturer's instructions. Library preparation — encompassing barcoding, reverse transcription, and amplification — was carried out subsequently. The snRNA-seq libraries were sequenced on an Illumina NovaSeq 6000 platform, generating 150 bp paired-end reads.

Primary analysis of raw read data

To generate gene expression profiles, raw reads were analyzed using CeleScope v2.0.7 (Singleron Biotechnologies) under default settings. Barcodes and UMIs were extracted and corrected from R1 reads, while adapter sequences and poly-A tails were removed from R2 reads, which were then aligned to the mRatBN7.2 (rattus_ensembl_111) transcriptome using STARsolo in STAR v2.7.11a. The key parameters for STARsolo included `--outFilterMatchNmin 50`, whereas `--outFilterMismatchNmax` was kept at the default value of 10. Successfully assigned reads with identical cell barcodes, UMIs, and genes were combined to generate the gene expression matrix for subsequent analyses.

Quality control, dimension-reduction and clustering

For each sample dataset, cells and genes were filtered based on the following thresholds: cells with <200 genes or in the top 2% of gene counts, cells in the top 2% of UMI counts, cells with >10% mitochondrial content, and genes expressed in fewer than 5 cells were excluded. After filtering, 71,831 cells remained for subsequent analyses, averaging 3,285 genes and 1,409 UMIs per cell. The raw counts were normalized per cell and log-transformed to produce the normalized expression matrix. Using `flavor = 'seurat'`, the top 2,000 variable genes were selected, and PCA was applied to the scaled matrix, with the top 20 components employed for clustering and dimensional reduction. Data integration and batch effect correction were performed using the Harmony algorithm¹⁶. Using the Louvain algorithm with a resolution of 1.2, cells were partitioned into 22 clusters. We visualized cell clusters using UMAP, performing the final

visualization on the batch-corrected dataset to confirm that the observed clustering represented genuine biological variation. Quality control, dimensionality reduction, and clustering were performed using Scanpy v1.8.2.

Differentially expressed genes (DEGs) analysis

We defined genes as differentially expressed if they were expressed in more than 10% of cells within a cluster and had an average log (Fold Change) exceeding 0.25. For cell-type annotation, canonical marker genes among the DEGs were cross-referenced with relevant literature. DEGs were identified using the FindMarkers function in Seurat, applying the Wilcoxon rank-sum test with default parameters. Doublet cells, characterized by the co-expression of markers from multiple cell types, were manually identified and excluded from further analysis.

Cell type annotation

Cell type identities for each cluster were determined by integrating the expression of canonical marker genes identified among the DEGs with information from the SynEcoSys database. The expression patterns of these marker genes were visualized using heatmaps, dot plots, and violin plots generated with the DoHeatmap, DotPlot, and VlnPlot functions in Seurat v3.1.2.

Pathway enrichment analysis

We performed Gene Ontology (GO) and Kyoto Encyclopedia of Genes and Genomes (KEGG) analyses¹⁷⁻¹⁹ using the clusterProfiler R package (v3.16.1) to investigate the potential functions of the DEGs. All KEGG-related figures were

generated by the authors based on pathway annotation and enrichment results, without reproducing KEGG pathway maps or original KEGG database images. Pathways with $p\text{-adj} < 0.05$ were regarded as significantly enriched, and GO gene sets were analyzed across MF, BP, and CC categories.

Statistical Analysis

Data are presented as mean \pm standard deviation (SD). Comparisons between two groups were performed using an unpaired Student's t-test, with $p < 0.05$ considered statistically significant. Statistical analyses were conducted using GraphPad Prism (version 8.0.1; GraphPad Software, San Diego, CA, USA; <https://www.graphpad.com>).

Results

Effect of CIH on rat liver histology

To investigate the effect of CIH on rat liver at both the cellular and histological levels, we performed snRNA-seq and histological analysis. The overall study workflow is illustrated in Figure 1A. Liver tissues were collected from rats in the NC and CIH groups, and snRNA-seq was performed. Downstream analyses included quality control, data normalization, feature selection, cell annotation, dimensionality reduction, clustering to construct a single-nucleus atlas, as well as differential expression and functional enrichment analyses. HE staining revealed clear histological differences between the groups (Figure 1B). In the NC group, liver architecture remained intact, with regularly arranged hepatocytes and no evident inflammatory infiltration or structural

abnormalities. By contrast, livers from CIH-exposed rats exhibited marked histological changes, including spotty necrosis within hepatic lobules (arrow, lower-left panel) and prominent inflammatory cell infiltration mainly restricted to portal tracts (arrow, lower-right panel). These results indicate that CIH induces marked histological changes in rat liver.

Impact of CIH on the single-nucleus transcriptomic landscape of rat liver

After quality control filtering, we obtained 37,973 and 33,858 high-quality single nuclei from the NC and CIH groups, respectively. We distinguished and characterized ten liver cell populations by unsupervised clustering analysis, including Hepatocytes, Endothelial cells (ECs), Fibroblasts, Mural cells (predominantly hepatic stellate cells, HepSCs), Plasma cells, B cells, T and NK cells, Neutrophils, Mononuclear phagocytes (MPs), Plasmacytoid dendritic cells (pDCs) (Figure 2A-C). In Figure 2D and E, the top 10 and top 3 DEGs across all cell types were displayed, highlighting the distinct transcriptomic features of the ten cell types. Additionally, we analyzed the proportion changes in each hepatic cell subpopulation between the two groups. The results demonstrated that the main cell type in rat liver tissue remained proportionally stable, and the proportions of other immune and stromal cells also didn't change (Figure 2F-G). In addition to these major populations, a small epithelial subset expressing cholangiocyte-associated markers (Cftr, Epcam, Krt7, Mmp7, and Sox9) was observed and visualized by FeaturePlot analysis (Supplementary Figure S1).

Hepatocytes and HepSCs

Next, we investigated the impact of CIH on hepatocytes. Eight hepatocytes subpopulations were identified, including Hepatocytes_Cxcl1, Hepatocytes_Cyp7a1, Hepatocytes_Igfbp1, Hepatocytes_Mt - atp6, Hepatocytes_Obp3, Hepatocytes_Pigr, Hepatocytes_Slc27a2, and Hepatocytes_Slc7a2 (Figure 3A, B). After CIH treatment, the proportions of Hepatocytes_Mt - atp6, Hepatocytes_Obp3, and Hepatocytes_Pigr subpopulations declined, while those of Hepatocytes_Cxcl1, Hepatocytes_Cyp7a1, Hepatocytes_Igfbp1, Hepatocytes_Slc27a2, and Hepatocytes_Slc7a2 subpopulations increased (Figure 3C). The most significant DEGs among hepatocytes subpopulations were visually depicted in Figure 3D-E. GO and KEGG pathway analyses of these DEGs are presented in Figure 3F - I. The up-regulated DEGs were primarily enriched in KEGG pathways involved in Complement and coagulation cascades, glycine, serine and threonine metabolism, and AMPK signaling pathway (Figure 3H). The down-regulated DEGs were mainly enriched in KEGG pathways related to metabolic processes (e.g., insulin resistance, fatty acid metabolism, and steroid hormone biosynthesis) and signaling/transduction and stress responses (e.g., PPAR signaling pathway and chemical carcinogenesis) (Figure 3I).

HepSCs were clustered into five main subgroups: HepSCs_Itm2b, HepSCs_Mt-co1, HepSCs_Oca2, HepSCs_Svep1, and HepSCs_Thbs1 (Figure 4A, B). Differences in subpopulation distribution existed between the NC and CIH groups (Figure 4C). The most representative DEGs in the HepSCs

subpopulations are visualized in Figure 4D, E. Furthermore, we performed an enrichment analysis to explore the functional characteristics of HepSCs (Figure 4F - I). KEGG analysis showed that up-regulated DEGs in HepSCs subpopulations were linked to PI3K - Akt and cGMP - PKG signaling pathways, focal adhesion, and collagen - receptor interaction (Figure 4H) while down-regulated DEGs were associated with fatty acid metabolism, steroid hormone biosynthesis, the PPAR signaling pathway, and chemical carcinogenesis-DNA adducts, etc (Figure 4I).

MPs and ECs

Cluster analysis of hepatic MPs revealed seven subpopulations: Kupffer cells (KCs), Monocytes, cDC1, cDC2, (Figure 5A, B), with KCs constituting the predominant component. This aligns with their role as the primary resident macrophages in liver sinusoids. Differences in the clustering distribution between the NC and CIH groups were observed (Figure 5C). Figure 5D and E show the most significantly DEGs in the MPs subpopulations. Results of GO and KEGG analyses are presented in Figure 5F - H. Up-regulated DEGs were associated with the complement and coagulation cascades, NF-kappa B signaling pathway and AMPK signaling pathway (Figure 5H).

Three distinct ECs subpopulations were identified: arterial ECs (AECs), liver sinusoidal ECs (LSECs), and venous ECs (VECs) (Figure 6A, B). It was found that the NC and CIH groups had different clustering distribution (Figure 6C). Figure 6D and E visually illustrate the most significant DEGs in ECs. Functional enrichment analysis was performed to clarify the biological functions (Figure 6F

- I). Up-regulated DEGs were primarily enriched in Complement and coagulation cascades, Primary bile acid biosynthesis, Fatty acid degradation, and cytochrome P450, etc (Figure 6H). Down-regulated DEGs were primarily associated with the KEGG pathways associated with leukocyte transendothelial migration, tight junction, platelet activation, and Hippo signaling pathway, etc (Figure 6I).

T cell

Three distinct T cell subpopulations were identified, which showed different proportional distributions (Figure 7A-C). The most significant DEGs in T cells are shown in Figure 7D, E. The molecular functions, cellular components, biological processes, and KEGG pathways of T cells are presented in Figure 7F-I. KEGG pathway analysis indicated that up-regulated DEGs were enriched in pathways such as complement and coagulation cascades, nicotinate and nicotinamide metabolism and steroid hormone biosynthesis (Figure 7H), while down-regulated DEGs were associated with Antigen processing and presentation, Estrogen signaling pathway, and Protein processing in endoplasmic reticulum (Figure 7I).

Discussion

This study utilized snRNA-seq to comprehensively investigate the impact of CIH on the liver in a rodent model. The results demonstrated significant alterations in both pathological histology and the functional characteristics of the liver microenvironment following CIH exposure. Histological analysis revealed that CIH induced substantial liver injury, characterized by spotty necrosis accompanied by prominent infiltration of inflammatory cells. Transcriptomic

profiling identified 10 distinct liver cell types; however, the composition of these clusters showed no change under CIH conditions. This lack of shift may be associated with the liver's robust metabolic adaptability and compensatory mechanisms. Subpopulation analysis further unveiled cell-type-specific transcriptional changes across various liver cell populations. Key findings include: suppression of PPAR signaling pathway and fatty acid metabolism in hepatocytes and HepSCs, inflammatory activation and enhanced oxidative stress in KCs, disassembly of the endothelial cytoskeleton and disruption of cellular junctions in ECs. These findings provide crucial insights into the complex interplay between CIH and the liver microenvironment and identify potential novel therapeutic targets.

A growing body of evidence indicates an association between OSA and liver injury. Krolow et al.²⁰ demonstrated moderate-to-severe OSA is associated with an increased risk of developing liver fibrosis, independent of obesity. A retrospective study of 410 individuals revealed that OSA severity is a risk factor for NAFLD and liver fibrosis²¹. Furthermore, in our analysis of 19,362 participants, the presence of sleep apnea was significantly correlated with elevated liver enzymes and liver steatosis, and a dose-response relationship was observed between sleep apnea severity and these liver alterations²². These results collectively demonstrate a robust and autonomous link between OSA and deterioration of liver function in populations.

Prior studies have established a link between CIH and hepatic injury in

animal models^{4,5,23}. In a study exposing rats to combined high-fat diet and CIH conditions, CIH exposure for 9 weeks significantly increased serum transaminases and myeloperoxidase levels compared to high-fat diet controls without CIH. Histological analysis further revealed evidence of hepatic inflammation and fibrosis²³. Savransky V et al.⁵ demonstrated that CIH induced hepatocyte swelling, lobular spotty necrosis, and enhanced activity of hepatocyte nuclear factor (NF)- κ B. Additionally, CIH markedly exacerbated acetaminophen-induced hepatotoxicity, leading to fulminant hepatocellular injury. Another investigation indicated that CIH may provoke hepatic injury in rats through oxidative stress, concomitant with activation of the pro-inflammatory transcription factor NF- κ B. Notably, the antioxidant tempol attenuated CIH-induced liver damage by counteracting oxidative stress^{Error! Reference source not found.}. Collectively, these findings implicate OSA and its associated CIH in the pathogenesis of liver injury. Consistent with these reports, our study confirms that CIH exposure induces hepatic injury characterized by hepatocyte necrosis accompanied by prominent infiltration of inflammatory cells. Concomitantly, through snRNA-seq, we dissected gene expression profiles at the individual cell level across hepatic subpopulations. This approach enables more precise delineation of the molecular mechanisms underlying CIH-induced hepatic pathology.

Our study indicates that CIH exposure significantly affects hepatocytes and HepSCs. CIH altered hepatocyte transcriptional profiles, promoting stress

response and energy regulation (complement/coagulation cascades, AMPK signaling) while suppressing key metabolic functions (insulin resistance, fatty acid metabolism, PPAR signaling), which may be involved in liver dysfunction under CIH. Our finding that the AMPK signaling pathway is significantly up-regulated in hepatocyte subpopulations after CIH exposure is consistent with previous reports showing hypoxia-induced AMPK activation in multiple tissues including liver²⁴. Moreover, the observed enrichment of glycine, serine and threonine metabolism pathways aligns with transcriptomic and metabolomic evidence of amino acid metabolic disturbance in the liver under chronic hypoxia²⁵. In addition, hypoxia has been shown to inhibit hepatic PPAR α via ERK signaling, leading to impaired fatty acid β -oxidation and promoting fatty liver²⁶. Our enrichment results showing up-regulation of PI3K-Akt, focal adhesion and collagen-receptor interaction pathways in HepSC subpopulations align with prior work on HepSC activation and liver fibrosis, where PI3K/Akt signaling is essential for HepSCs proliferation and extracellular matrix (ECM) production. A study found that inhibition of PI3K in HepSCs reduced collagen expression and migration²⁷. Moreover, focal adhesion components such as FAK, vinculin and talin are significantly increased during HepSCs activation, facilitating increased cell-matrix interaction and ECM remodeling^{28,29}. Conversely, reduced fatty acid metabolism and PPAR signaling observed in our data align with previous studies linking impaired PPAR α activity to hepatic lipid dysregulation and fibrogenesis, suggesting a potential association between metabolic alterations in HepSCs and

disease progression³⁰. Taken together, these data support a model in which HepSCs under fibrogenic stress shift from metabolic maintenance functions toward pro-fibrotic, matrix-remodeling programs.

MPs exhibited abnormal activation of complement/coagulation cascades and NF- κ B signaling, suggesting a pro-inflammatory and pro-coagulant transcriptional profile that may be associated with CIH-related liver injury and fibrosis. Hepatic macrophage NF- κ B activation was shown to induce liver fibrosis^{31,32}, and macrophage AMPK signaling has been linked to regulation of macrophage metabolism and inflammation³³. Up-regulated DEGs in liver endothelial cells were enriched in fatty acid degradation and cytochrome P450 pathways, consistent with the unique metabolic and detoxification functions of LSECs³⁴. Down-regulated DEGs were associated with leukocyte transendothelial migration, tight junction, and Hippo signaling pathways, reflecting alterations in endothelial barrier function and signaling that may impact immune cell trafficking and endothelial-mesenchymal transition during liver stress^{35,36}. Our observation that up-regulated DEGs in T cell subpopulations are enriched in complement and coagulation cascades is in line with the established role of complement in bridging innate and adaptive immunity³⁷. Meanwhile, the down-regulation of genes in endoplasmic reticulum (ER) protein processing pathways may reflect suppressed unfolded protein response (UPR) or ER stress tolerance in T cells under stress, consistent with the literature showing that ER stress modulates T cell activation and effector function³⁸. Together, these results

suggest that these T cell subgroups might undergo both immune regulatory shifts and metabolic/ER stress adaptations under experimental conditions.

To the best of our knowledge, this is the first study employing a snRNA-seq-based transcriptomic approach to investigate the pathophysiological mechanisms underlying CIH-induced liver injury. However, several limitations should be noted. First, the experimental design and findings were based on a rodent model of CIH, which may not fully capture the complexity of human OSA and liver injury comorbidities. Second, the analysis focused on transcriptomic data; further studies incorporating proteomic and metabolomic analyses are necessary to fully elucidate the underlying mechanisms. Third, although differentially expressed genes and related pathways were identified, our findings are hypothesis-generating in nature, and functional and mechanistic studies will be required to establish causal links between these transcriptional alterations and CIH-associated hepatic dysfunction. Finally, given the limited number of biological replicates, analyses of cell subpopulation proportions were intended to provide descriptive insights rather than formal statistical inference.

In conclusion, this study established a snRNA-seq transcriptomic atlas of the liver under CIH, systematically revealing dynamic remodeling features in hepatocytes and immune cells. By precisely identifying injury patterns and immune activation states in specific cell types during CIH exposure, it provides a pivotal theoretical foundation for the molecular mechanisms underlying OSA-associated liver injury. These discoveries not only offer deeper insights into

the pathological mechanisms of OSA-related liver damage at the cellular level but also lay the scientific groundwork for developing targeted therapeutic strategies to alleviate CIH-induced hepatic dysfunction.

Acknowledgements

The authors thank the Singleron Biotechnologies for their help with the single-nucleus RNA sequencing analysis. We sincerely thank Dr. Ningfang Lian from The First Affiliated Hospital of Fujian Medical University for providing assistance with the animal experiments.

Author Contributions

LDC supervised and designed this project. WSH, CQW, and JFH performed the animal experiment. JML and CDY prepared samples for snRNA-seq. WSH, LDC and LL analyzed the snRNA-seq data. YZH performed pathology analysis. WSH and CQW wrote the manuscript.

Availability of data and materials

The single-nucleus RNA sequencing datasets generated and analyzed in this study have been deposited in the NCBI Sequence Read Archive (SRA) under accession number PRJNA1345096 and are publicly available at: <https://www.ncbi.nlm.nih.gov/sra/PRJNA1345096>.

Ethics statement

This study was approved by the approved by the Animal Ethics Committee of Fujian Medical University (IACUC FJMU 2022-0031). All methods were carried

out in accordance with relevant guidelines and regulations. All methods are also reported in accordance with ARRIVE guidelines.

Consent for publication

Not applicable.

Competing interests

The authors declare that they have no known competing financial interests or personal relationships that could have appeared to influence the work reported in this paper.

Funding

This work was supported by Natural Science Foundation of Fujian Province (2022J011474), Young people training project from Fujian Province Health Bureau (2022GGA053), and Startup Fund for Scientific Research of Fujian Medical University (2024QH1637), and grant PDA202202 for scientific research of Zhangzhou Affiliated Hospital of Fujian Medical University.

References

- 1 Benjafield, A. V. *et al.* Estimation of the global prevalence and burden of obstructive sleep apnoea: a literature-based analysis. *Lancet Respir Med* **7**, 687-698, doi:10.1016/S2213-2600(19)30198-5 (2019).
- 2 Mesarwi, O. A., Loomba, R. & Malhotra, A. Obstructive Sleep Apnea, Hypoxia, and Nonalcoholic Fatty Liver Disease. *Am J Respir Crit Care Med* **199**, 830-841, doi:10.1164/rccm.201806-1109TR (2019).
- 3 Wang, L. *et al.* Association of Obstructive Sleep Apnea with Nonalcoholic Fatty Liver Disease: Evidence, Mechanism, and Treatment. *Nat Sci Sleep* **16**, 917-933, doi:10.2147/NSS.S468420 (2024).
- 4 Savransky, V. *et al.* Chronic intermittent hypoxia causes hepatitis in a mouse model of diet-induced fatty liver. *Am J Physiol Gastrointest Liver Physiol* **293**, G871-877, doi:10.1152/ajpgi.00145.2007 (2007).
- 5 Savransky, V. *et al.* Chronic intermittent hypoxia predisposes to liver injury. *Hepatology* **45**, 1007-1013, doi:10.1002/hep.21593 (2007).
- 6 Chen, L. D. *et al.* Effect of chronic intermittent hypoxia on gene expression profiles of rat liver: a better understanding of OSA-related liver disease. *Sleep Breath* **24**, 761-770, doi:10.1007/s11325-019-01987-0 (2020).
- 7 Kim, N., Kang, H., Jo, A., Yoo, S. A. & Lee, H. O. Perspectives on single-nucleus RNA sequencing in different cell types and tissues. *J Pathol Transl Med* **57**, 52-59, doi:10.4132/jptm.2022.12.19 (2023).

- 8 Hicks, S. C., Townes, F. W., Teng, M. & Irizarry, R. A. Missing data and technical variability in single-cell RNA-sequencing experiments. *Biostatistics* **19**, 562-578, doi:10.1093/biostatistics/kxx053 (2018).
- 9 Haque, A., Engel, J., Teichmann, S. A. & Lonnberg, T. A practical guide to single-cell RNA-sequencing for biomedical research and clinical applications. *Genome Med* **9**, 75, doi:10.1186/s13073-017-0467-4 (2017).
- 10 Minati, M. A., Fages, A., Dauguet, N., Zhu, J. & Jacquemin, P. Optimized nucleus isolation protocol from frozen mouse tissues for single nucleus RNA sequencing application. *Front Cell Dev Biol* **11**, 1243863, doi:10.3389/fcell.2023.1243863 (2023).
- 11 Gao, R. *et al.* Nanogrid single-nucleus RNA sequencing reveals phenotypic diversity in breast cancer. *Nat Commun* **8**, 228, doi:10.1038/s41467-017-00244-w (2017).
- 12 Li, X. Y. *et al.* Single-nucleus RNA sequencing uncovers metabolic dysregulation in the prefrontal cortex of major depressive disorder patients. *Sci Rep* **15**, 7418, doi:10.1038/s41598-025-92030-8 (2025).
- 13 Lau, S. F., Cao, H., Fu, A. K. Y. & Ip, N. Y. Single-nucleus transcriptome analysis reveals dysregulation of angiogenic endothelial cells and neuroprotective glia in Alzheimer's disease. *Proc Natl Acad Sci U S A* **117**, 25800-25809, doi:10.1073/pnas.2008762117 (2020).
- 14 Lee, S. H. T. *et al.* Single nucleus RNA-sequencing integrated into risk variant colocalization discovers 17 cell-type-specific abdominal obesity

- genes for metabolic dysfunction-associated steatotic liver disease. *EBioMedicine* **106**, 105232, doi:10.1016/j.ebiom.2024.105232 (2024).
- 15 Chen, J. *et al.* 2-Methoxyestradiol attenuates lung injury induced by chronic intermittent hypoxia via inhibiting the HIF1-alpha/SLC7A11 pathway. *Sci Rep* **15**, 17601, doi:10.1038/s41598-025-02675-8 (2025).
- 16 Korsunsky, I. *et al.* Fast, sensitive and accurate integration of single-cell data with Harmony. *Nat Methods* **16**, 1289-1296, doi:10.1038/s41592-019-0619-0 (2019).
- 17 Kanehisa, M. & Goto, S. KEGG: kyoto encyclopedia of genes and genomes. *Nucleic Acids Res* **28**, 27-30, doi:10.1093/nar/28.1.27 (2000).
- 18 Kanehisa, M. Toward understanding the origin and evolution of cellular organisms. *Protein Sci* **28**, 1947-1951, doi:10.1002/pro.3715 (2019).
- 19 Kanehisa, M., Furumichi, M., Sato, Y., Matsuura, Y. & Ishiguro-Watanabe, M. KEGG: biological systems database as a model of the real world. *Nucleic Acids Res* **53**, D672-D677, doi:10.1093/nar/gkae909 (2025).
- 20 Krolow, G. K., Garcia, E., Schoor, F., Araujo, F. B. S. & Coral, G. P. Obstructive sleep apnea and severity of nonalcoholic fatty liver disease. *Eur J Gastroenterol Hepatol* **33**, 1104-1109, doi:10.1097/MEG.0000000000001920 (2021).
- 21 Lian, N. *et al.* Risk Factors of Nonalcoholic Fatty Liver Disease and Liver Fibrosis in Non-Obese Patients with Obstructive Sleep Apnea. *Nat Sci Sleep* **14**, 2143-2149, doi:10.2147/NSS.S388203 (2022).

- 22 Jiang, Y. B., Huang, Z. W., Lin, X. J., Luo, J. M. & Chen, L. D. Association between self-reported sleep apnea and biomarkers of liver injury: Evidence from National Health and Nutrition Examination Survey. *Medicine (Baltimore)* **103**, e39393, doi:10.1097/MD.00000000000039393 (2024).
- 23 Feng, S. Z. *et al.* An experimental research on chronic intermittent hypoxia leading to liver injury. *Sleep Breath* **15**, 493-502, doi:10.1007/s11325-010-0370-3 (2011).
- 24 Song, K., Zhang, Y., Ga, Q., Bai, Z. & Ge, R. L. High-altitude chronic hypoxia ameliorates obesity-induced non-alcoholic fatty liver disease in mice by regulating mitochondrial and AMPK signaling. *Life Sci* **252**, 117633, doi:10.1016/j.lfs.2020.117633 (2020).
- 25 Liang, H. & Song, K. Comprehensive metabolomics and transcriptomics analysis reveals protein and amino acid metabolic characteristics in liver tissue under chronic hypoxia. *PLoS One* **18**, e0291798, doi:10.1371/journal.pone.0291798 (2023).
- 26 Mooli, R. G. R. *et al.* Hypoxia via ERK Signaling Inhibits Hepatic PPARalpha to Promote Fatty Liver. *Cell Mol Gastroenterol Hepatol* **12**, 585-597, doi:10.1016/j.jcmgh.2021.03.011 (2021).
- 27 Son, G., Hines, I. N., Lindquist, J., Schrum, L. W. & Rippe, R. A. Inhibition of phosphatidylinositol 3-kinase signaling in hepatic stellate cells blocks the progression of hepatic fibrosis. *Hepatology* **50**, 1512-1523,

- doi:10.1002/hep.23186 (2009).
- 28 Zhao, X. K. *et al.* Focal Adhesion Kinase Regulates Hepatic Stellate Cell Activation and Liver Fibrosis. *Sci Rep* **7**, 4032, doi:10.1038/s41598-017-04317-0 (2017).
- 29 Hijazi, N., Shi, Z. & Rockey, D. C. Characterization of focal adhesion proteins in rodent hepatic stellate cells. *Histochem Cell Biol* **158**, 325-334, doi:10.1007/s00418-022-02123-y (2022).
- 30 Wang, Y., Nakajima, T., Gonzalez, F. J. & Tanaka, N. PPARs as Metabolic Regulators in the Liver: Lessons from Liver-Specific PPAR-Null Mice. *Int J Mol Sci* **21**, doi:10.3390/ijms21062061 (2020).
- 31 Sunami, Y. *et al.* Hepatic activation of IKK/NFkappaB signaling induces liver fibrosis via macrophage-mediated chronic inflammation. *Hepatology* **56**, 1117-1128, doi:10.1002/hep.25711 (2012).
- 32 El Kasmi, K. C. *et al.* Macrophage-derived IL-1beta/NF-kappaB signaling mediates parenteral nutrition-associated cholestasis. *Nat Commun* **9**, 1393, doi:10.1038/s41467-018-03764-1 (2018).
- 33 Cui, Y. *et al.* The role of AMPK in macrophage metabolism, function and polarisation. *J Transl Med* **21**, 892, doi:10.1186/s12967-023-04772-6 (2023).
- 34 Kaczara, P. *et al.* Liver sinusoidal endothelial cells rely on oxidative phosphorylation but avoid processing long-chain fatty acids in their mitochondria. *Cell Mol Biol Lett* **29**, 67, doi:10.1186/s11658-024-00584-8

- (2024).
- 35 Patten, D. A. *et al.* Human liver sinusoidal endothelial cells promote intracellular crawling of lymphocytes during recruitment: A new step in migration. *Hepatology* **65**, 294-309, doi:10.1002/hep.28879 (2017).
- 36 Zhou, Y. *et al.* Angiotensin II depends on hippo/YAP signaling to reprogram angiogenesis and promote liver fibrosis. *Cell Signal* **123**, 111355, doi:10.1016/j.cellsig.2024.111355 (2024).
- 37 Dunkelberger, J. R. & Song, W. C. Complement and its role in innate and adaptive immune responses. *Cell Res* **20**, 34-50, doi:10.1038/cr.2009.139 (2010).
- 38 Zhang, W. & Cao, X. Unfolded protein responses in T cell immunity. *Front Immunol* **15**, 1515715, doi:10.3389/fimmu.2024.1515715 (2024).

Legends

Figure 1. Effect of CIH on rat liver histology and single-nucleus transcriptomic analysis. (A) Experimental design and workflow for snRNA-seq analysis in rat liver, including group assignment, nuclei isolation, sequencing, quality control, normalization, feature selection, dimensionality reduction, clustering, cell annotation, and downstream analyses including differential gene expression and functional enrichment. (B) Representative hematoxylin and eosin staining of liver sections from NC and CIH groups. Scale bars = 50 μ m.

Figure 2 Overview of the 71,831 single nuclei isolated from the liver of NC and CIH rats (n=3). (A) UMAP plot of liver cell clusters colored by experimental group (NC vs. CIH), illustrating the distribution of cells from each group. (B) UMAP plot of liver cell clusters colored by each sample. (C) UMAP plot of liver cell clusters colored by distinct cell types (D) Heatmap showing the expression patterns of marker genes across different cell clusters. (E) Bubble plot of the top 3 DEGs among all cell types. (F) The proportion of cell subpopulations in the NC and CIH groups (G) Comparisons of cell subpopulation proportions between NC and CIH groups. Data are shown as the mean \pm SD. Statistical significance was determined using an unpaired two-tailed Student's t-test. "ns" indicates no significant difference.

Figure 3 Effects of CIH on hepatocyte subpopulations in rat liver (n=3). (A) UMAP plot showing eight hepatocyte subpopulations identified from snRNA-seq data: Hepatocytes_Cxcl1, Hepatocytes_Cyp7a1, Hepatocytes_Igfbp1,

Hepatocytes_Mt-atp6, Hepatocytes_Obp3, Hepatocytes_Pigr, Hepatocytes_Slc27a2, and Hepatocytes_Slc7a2. (B) UMAP plot showing hepatocytes derived from the NC and CIH groups. (C) Proportional distribution of hepatocyte subpopulations between the NC and CIH groups. (D) Heatmap showing the top DEGs across the eight hepatocyte subpopulations. (E) Violin plot showing the expression of representative marker genes in each hepatocyte subpopulation. (F) GO enrichment analysis of up-regulated DEGs in hepatocytes between the CIH and NC groups. (G) GO enrichment analysis of down-regulated DEGs in hepatocytes between the CIH and NC groups. (H) KEGG pathway enrichment analysis of up-regulated DEGs in hepatocytes. (I) KEGG pathway enrichment analysis of down-regulated DEGs in hepatocytes.

Figure 4 Effects of CIH on HepSC subpopulations in rat liver (n=3). (A) UMAP plot of clusters representing HepSC subpopulations, including HepSCs_Itm2b, HepSCs_Mt-co1, HepSCs_Oca2, HepSCs_Svep1, and HepSCs_Thbs1. (B) UMAP plot showing hepatic stellate cell derived from the NC and CIH groups. (C) Proportional distribution of HepSC subpopulations between the NC and CIH groups. (D) Heatmap showing the top DEGs across the HepSC subpopulations. (E) Violin plot showing the expression of representative marker genes in each HepSC subpopulations. (F) GO enrichment analysis of up-regulated DEGs in HepSCs between the CIH and NC groups. (G) GO enrichment analysis of down-regulated DEGs in HepSCs between the CIH and NC groups. (H) KEGG pathway enrichment analysis of up-regulated DEGs in HepSCs. (I) KEGG

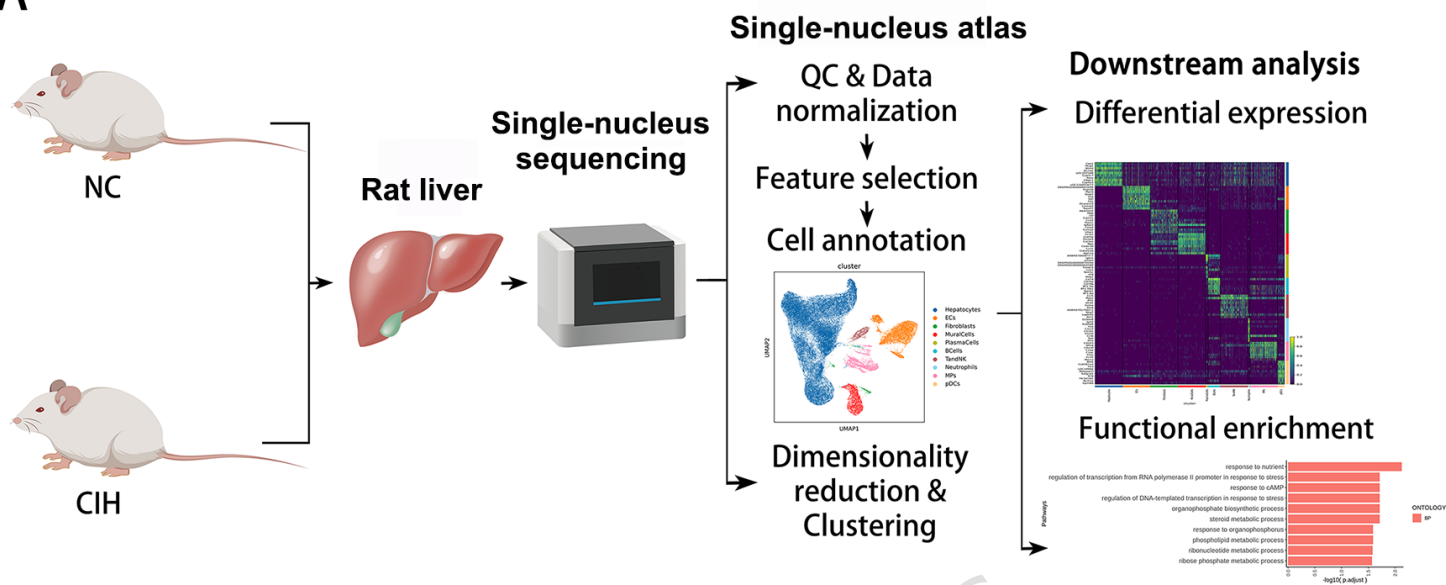
pathway enrichment analysis of down-regulated DEGs in HepSCs.

Figure 5 Effects of CIH on MP subpopulations in rat liver (n=3). (A) UMAP plot of clusters representing MP subpopulations, including KCs, Monocytes, cDC1, cDC2. (B) UMAP plot showing MPs derived from the NC and CIH groups. (C) Proportional distribution of MP subpopulations between the NC and CIH groups. (D) Heatmap showing the top DEGs across the MP subpopulations. (E) Violin plot showing the expression of representative marker genes in each MP subpopulations. (F) GO enrichment analysis of up-regulated DEGs in MPs between the NC and CIH groups. (G) GO enrichment analysis of down-regulated DEGs in MPs between the NC and CIH groups. (H) KEGG pathway enrichment analysis of up-regulated DEGs in MPs.

Figure 6 Effects of CIH on EC subpopulations in rat liver (n=3). (A) UMAP plot of clusters representing EC subpopulations, including AECs, LSECs, and VECs. (B) UMAP plot showing ECs derived from the NC and CIH groups. (C) Proportional distribution of EC subpopulations between the NC and CIH groups. (D) Heatmap showing the top DEGs across the EC subpopulations. (E) Violin plot showing the expression of representative marker genes in each EC subpopulations. (F) GO enrichment analysis of up-regulated DEGs in ECs between the CIH and NC groups. (G) GO enrichment analysis of down-regulated DEGs in ECs between the CIH and NC groups. (H) KEGG pathway enrichment analysis of up-regulated DEGs in ECs. (I) KEGG pathway enrichment analysis of down-regulated DEGs in ECs.

Figure 7 Effects of CIH on T cell subpopulations in rat liver (n=3). (A) UMAP plot of cells colored by cluster, identifying three T cell subpopulations: ProliferatingT, CD8NaiveT, and CD8Teff. (B) UMAP plot showing T cell derived from the NC and CIH groups. (C) Proportional distribution of T cell subpopulations between the NC and CIH groups. (D) Heatmap showing the top DEGs across the T cell subpopulations. (E) Violin plot showing the expression of representative marker genes in each T cell subpopulation. (F) GO enrichment analysis of up-regulated DEGs in T cell between the NC and CIH groups. (G) GO enrichment analysis of down-regulated DEGs in T cell between the NC and CIH groups. (H) KEGG pathway enrichment analysis of up-regulated DEGs in T cell. (I) KEGG pathway enrichment analysis of down-regulated DEGs in T cell.

A



B

